



Cu-Mn and Cu-Ce Supported over Agro-based Carbons: Characteristics and NO_x Adsorption Study

I. Yakub¹, N. Mohamed Sutan¹, K. A. Mohd Said¹, A. Anuar^{1,2}, T. Y. Yun Hin²

¹Faculty of Engineering, Universiti Malaysia Sarawak, Sarawak, Malaysia

²Catalysis Science and Technology Research Centre, Faculty of Science, Universiti Putra Malaysia, Selangor, Malaysia

Received 15 Dec 2015, Revised 04 Feb 2016, Accepted 16 Feb 2016

*Corresponding author: E-mail: yibrahim@feng.unimas.my (I. Yakub); Phone: +6082583264; Fax: +6082583410

Abstract

As there is an urgent need for cheaper and sustainable resources for selective catalytic reduction catalyst, this study determined the potential, in terms of the catalyst characteristics and NO_x adsorption, of coconut shell (CSAC) and palm kernel shell activated carbons (PSAC) to be used as precursors for the catalyst in a low-temperature flue gas denitrification system. The carbons were impregnated with bimetallic catalysts – copper-manganese (Cu-Mn) and copper-cerium (Cu-Ce) – before calcined at low temperature. The produced coconut shell catalysts (CuMn/CS and CuCe/CS) and palm kernel shell catalysts (CuMn/PS and CuCe/PS) were then characterized using a nitrogen adsorption-desorption test, Fourier-Transform infra-red, x-ray fluorescence, x-ray diffraction and hydrogen temperature-programmed reduction. The removal of NO_x was also studied for all catalysts in a fixed-bed reactor. It was found that CuMn/CS gave the highest NO_x removal. CuMn/CS had high pore volume, good Cu-Mn crystallinity, high metal loading and dispersion, high copper reduction activity at the operating temperature, and rich in ketone and amine surface functional groups. It is then concluded that the coconut shell has the potential to be developed as a good SCR catalyst via impregnation with Cu-Mn.

Keywords: Selective Catalytic Reduction, NO_x adsorption, characterization, coconut shell carbon, palm kernel shell carbon

1. Introduction

Biomass valorization is a relatively new model in promoting the principle of sustainable development. The three-fold benefits of valorizing the abundant local agriculture-generated by-products are energy sustainability as well as reducing environmental and economic impacts [1]. In other words, agro-wastes are cost-effectively renewable, accessible and available. Until 2013, the world crops waste generated from the coconut production was more than 2.4 million tonnes per annum while palm kernels contributed to almost 10,000 tonnes waste per year [2]. Even though these agro-wastes are not classified as hazardous materials, the current practices of biomass disposal in developing countries are dumping in landfill and open burning; these caused serious risk to the environment and society [3].

The abundant agro-wastes are highly carbonaceous and low in inorganic contents. These characteristics make them the best option and suitable materials for activated carbons [3]. This fits in the valorization model since activated carbons from agro-wastes are more cost-effective, sustainable and energy efficient than the widely used commercial activated carbons. In a study by Singh et al. (2013), they utilized cotton stalks as catalysts for the selective catalytic reduction (SCR) [4]. This process is used to treat flue gases by converting nitrogen oxides into nitrogen over a catalyst capable of selectively reduces NO_x. The chemically activated cotton stalk possessed a

high BET surface area ranging from 826 to 1184 m²/g with an average pore size of 2.7 to 5.25 nm which surpassed other conventional catalyst supports. However, the catalyst had a moderate NO conversion at 66% compared to other metallic-supported catalysts that can achieve as high as 99% NO conversion [4]. Even though this is relatively low, it is still early to conclude that agro-waste catalysts cannot be competitive as biomass-derived activated carbons have lack of exploration as a catalyst support in the SCR.

As important as the support is, the catalyst used plays important roles in an SCR process. Metal nanoparticles such as copper, manganese and cerium are attractive candidates to be used as catalysts due to their large surface-to-volume ratio compared to bulk materials as shown in recent studies [5, 6]. A study also showed that bimetallic catalysts performed outstandingly in comparison to the monometallic ones [7]. This is due to the synergistic effects posed by the metals individually and as a couple. For instance, while one of the catalysts contributes to the Bronsted acid sites and the other increases the Lewis acid sites, together the catalysts can act as activators to the gaseous oxygen for use in an SCR reaction [8]. Among the reported synergistic effects between two metals are those of cerium-tungsten [8], manganese-cobalt [9], manganese-cerium [4], manganese-copper [10], cerium-zirconium [11], iridium-ruthenium [12] and silver-gold [13].

The most important ability for an SCR catalyst is the NO_x adsorption where there were direct correlations between the adsorption and the SCR performance [8, 14, 15, 16]. Therefore, it is the motivation of this study to explore the potential of bimetallic impregnated catalysts over agro-based carbons derived from coconut shells and palm kernel shells in terms of NO_x adsorption.

2. Experimental

2.1. Catalyst Synthesis

The synthesis of a NO_x-SCR catalyst involved three steps: (1) pretreatment of the catalyst support i.e. coconut shell carbon (CSAC) and palm kernel shell carbon (PSAC), (2) deposition of bimetallic catalysts (Cu-Mn and Cu-Ce) onto the support, and (3) calcination of the catalyst. The first step involved washing thoroughly of the CSAC and PSAC to remove impurities and drying in a 100 °C oven. Then, the coupled catalysts (Cu-Mn and Cu-Ce) were deposited onto the carbons using wet impregnation method described in [17]. Finally, the impregnated samples were calcined at 250 °C for 8 h and let to cool in a vacuumed desiccator. The abbreviation of the catalysts is shown in Table 1.

Table 1: List of catalysts synthesized and labels.

Precursor	Bimetallic catalysts	Abbreviation
CSAC	Cu-Mn	CuMn/CS
	Cu-Ce	CuCe/CS
PSAC	Cu-Mn	CuMn/PS
	Cu-Ce	CuCe/PS

2.2. Characterization Experiments

The catalysts were characterized to obtain the surface area properties, surface functional groups, metal loading and distribution, crystallinity and reducibility.

For the surface area analysis, approximately 0.7 g of the samples was put into a Chemisorb quartz tube and the nitrogen gas was allowed to flow over the particles at 77 K. This experiment was performed using an Autosorb Automated Gas Sorption system (Quantachrome Corporation, USA). The amount of nitrogen molecules adsorbed was correlated to the total surface area of the particles using the Brunauer-Emmett-Teller method.

A Fourier Transform infra-red spectrometer Thermo Nicolet 380 (Thermo Scientific Corporation, USA) was used to determine the surface functional groups present at the carbons and the catalysts. A beam of light that was a combination of many different frequencies was directed on the sample many times and the transmitted light was recorded as the light transmittance for each wavelength.

The metal loading and distribution were determined using the x-ray fluorescence technique. The samples were exposed to an x-ray radiation in an EDX-720/800HS Energy Dispersive X-ray Fluorescence spectrometer (Shimadzu Corporation, Japan). A set of energy level was released and each of the charge density refers to a

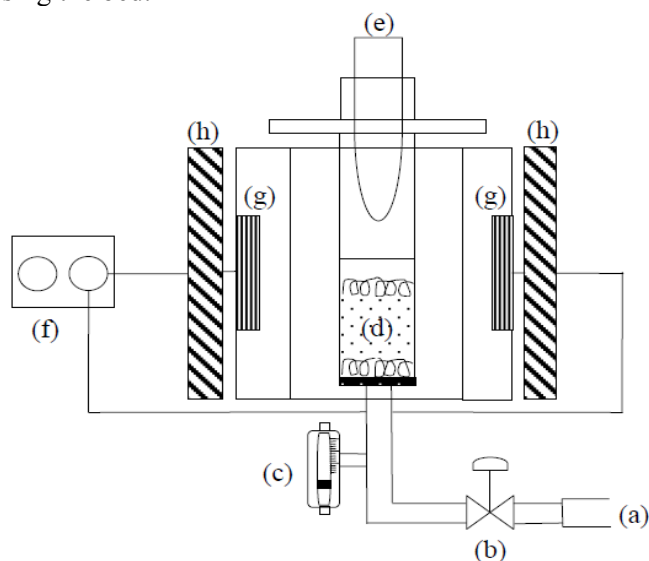
specific type of metal in the sample. This was repeated for several times over the sample surfaces and the standard deviation was taken as the distribution of the metals.

An x-ray diffractometer D/MAX rA (Rigaku Corporation, Japan) was used to analyze the crystallinity of the catalysts supported on different precursors. A monochromatic beam was projected onto the samples between 10 to 70 2-theta angle and the unique pattern of the reflection was plotted to describe the crystal phase of the metals.

The catalysts reducibility was examined using the hydrogen-temperature programmed reduction technique. This experiment was conducted using a Thermo Finnigan TPDRO 1100 (Thermo Scientific Corporation, USA) provided with a thermal conductivity detector. Prior to analysis, 20 mg of the catalysts were placed inside a quartz tube reactor and pretreated under a nitrogen stream at 150 °C for 10 min at 30 mL/min. After cooled to ambient temperature, the 5 %vol. H₂ in argon gas was introduced at 25 mL/min at elevated temperature until 950 °C with a ramp of 10 °C/min. In the meantime, the hydrogen consumption was measured at the effluent gas using the thermal conductivity detector.

2.3. Adsorption Study

An experimental set up was prepared as shown in Figure 1. Approximately 25 g of catalysts was placed inside the reactor and the bed was pre-heated to 100 °C. Then, a hot exhaust gas containing NO_x (136 ppm NO and 127 ppm NO₂) was connected to the reactor and let to flow at 5 std L/min. The temperature of the reactor was increased to 250 °C. The concentration of NO and NO₂ were detected using a gas analyzer Testo 350 XL (Testo Inc., Germany) before and after passing the bed.



(a) Exhaust pipe (b) Control valve (c) Flowmeter (d) Catalyst bed
 (e) Gas analyzer & temperature sensor (f) Temperature control
 (g) Heating elements (h) Protective casing

Figure 1: Schematic diagram of the fixed-bed reactor used for adsorption study.

The adsorption was correlated to the removal percentage that was calculated using equation (1);

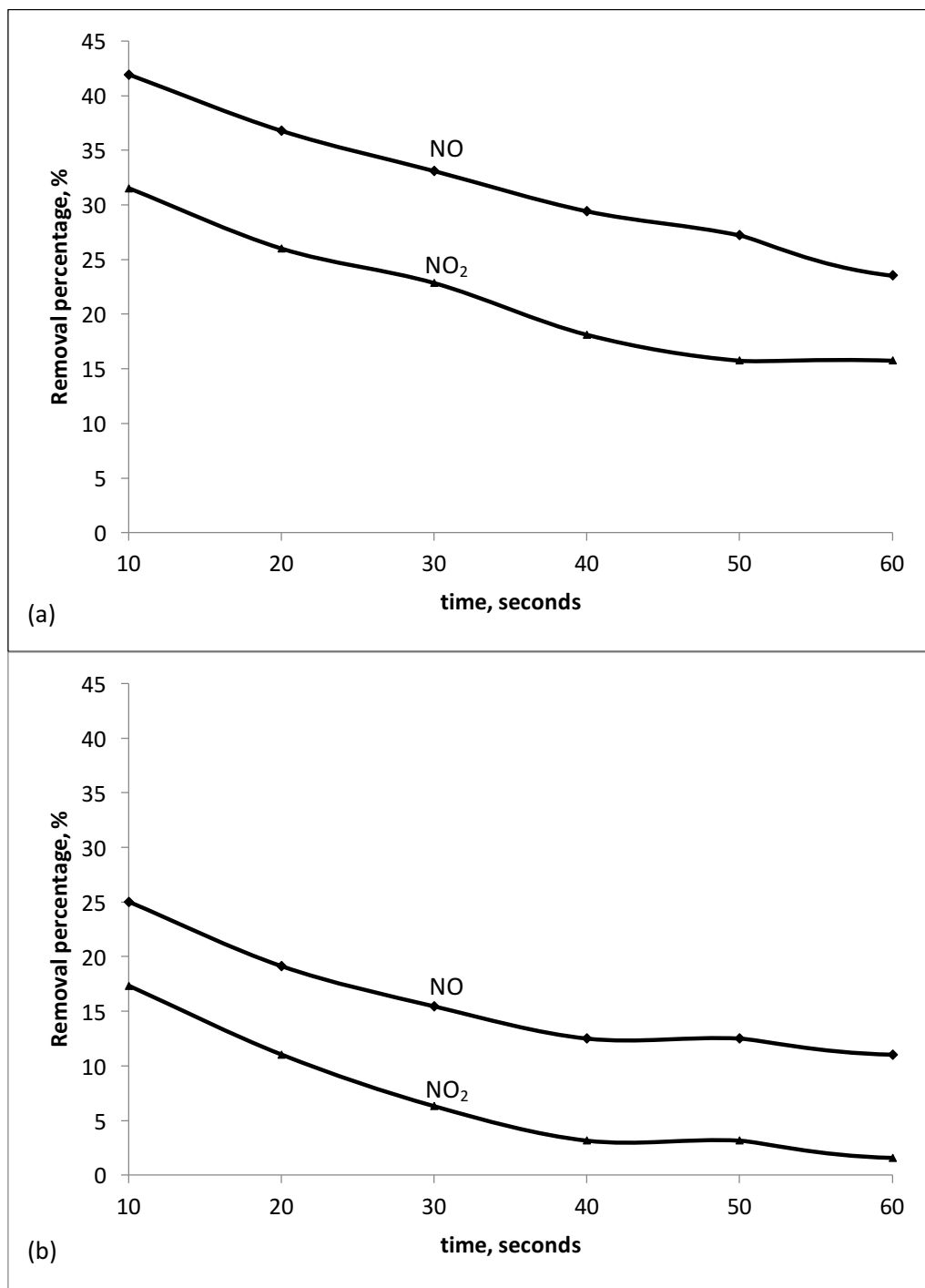
$$\text{Removal \%} = \frac{(NOx)_{initial} - (NOx)_{final}}{(NOx)_{initial}} \times 100\% \quad \dots\dots\dots(1)$$

where, $(NOx)_{initial}$ is the initial concentration of NO_x species (NO and NO₂) at the inlet (ppm), and $(NOx)_{final}$ is the final concentration of NO_x species at the outlet (ppm).

3. Results and discussion

3.1. Removal of NO_x gases

The performance of the synthesized catalysts in removing NO_x was analyzed based on the change in the concentration of NO_x in the flue gas at the inlet and outlet of a fixed-bed reactor. Figure 2 shows the removal percentage for NO_x when different catalysts were installed in the reactor.



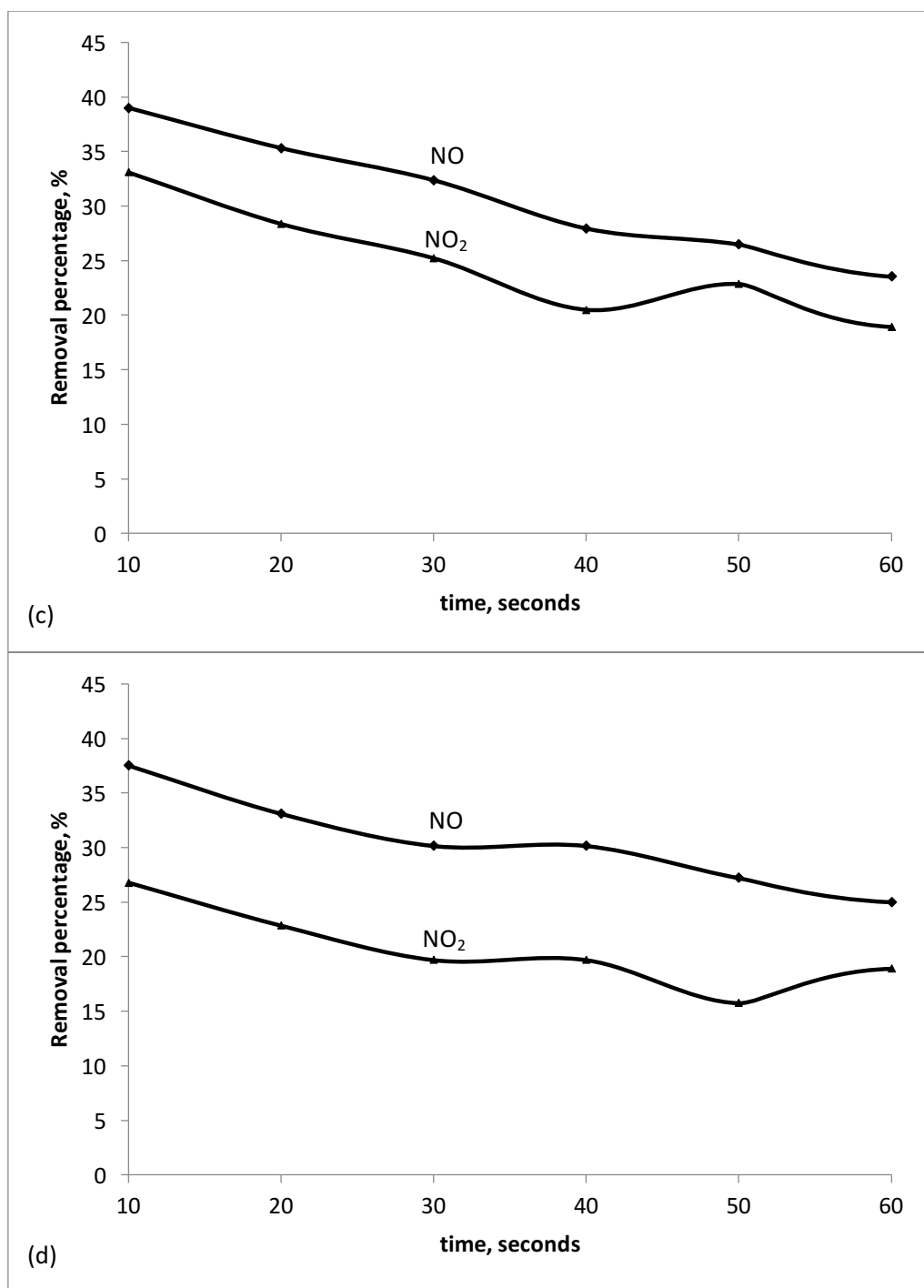


Figure 2: NO and NO₂ reduction profile for (a) CuMn/CS (b) CuCe/CS (c) CuMn/PS (d) CuCe/PS at 2.3 s⁻¹.

CuMn/CS exhibited the highest total NO_x gases removal, 74% (42% NO and 32% NO₂) followed by CuMn/PS (72%), CuCe/PS (65%) and CuCe/CS (42%). The performances between CuMn/CS and CuMn/PS were almost equivalent except that CuMn/CS removed more NO while CuMn/PS removed NO₂ the most. Besides, it was evident that CuCe impregnated catalysts removed less NO_x than the CuMn-based catalysts especially when the support used was coconut shell.

However, Muniz et al. (2000) compared the NO reduction rate by several origins of activated carbon and found that the coconut shell was among the highest when treated with sulfuric acid [18]. Bingnan et al. (2011) also concluded that coconut shells impregnated with Cu and K had the highest potential to be further developed as SCR catalysts where they claimed that the NO reduction can be as high as 95% [19]. Therefore, it can be deduced from this current study that the synergistic effect between Cu and Mn was better compared to Cu and Ce when incorporated onto PSAC and CSAC. The removal behavior was also consistent with the effect which was due to the characteristics of the catalysts that are discussed in the following sections.

3.2. Surface Area Analysis

The performance of a catalyst is influenced by its surface properties. Table 2 shows the surface area analysis of the raw catalyst supports and the derivative catalysts. As a catalyst support, PSAC had larger surface area compared to CSAC, therefore both CuMn/PS and CuCe/PS possessed larger surface area than the CSAC-supported catalysts.

Table 2: Surface and pore properties of CSAC, PSAC, CuMn/CS, CuCe/CS, CuMn/PS, CuCe/PS.

Properties	CSAC	CuMn/CS	CuCe/CS	PSAC	CuMn/PS	CuCe/PS
BET surface area (m ² /g)	819	903	503	1126	914	613
Micro pore volume (cc/g)	0.42	0.45	0.20	0.36	0.37	0.24
Average pore diameter (Å)	21	26	18	18	18	17

In this study, the BET surface area of the catalyst did not correlate proportionally to the performance. This was because the decreasing order of removal performance – CuMn/CS > CuMn/PS > CuCe/PS > CuCe/CS – did not match the decreasing order of the BET surface area – CuMn/PS > CuMn/CS > CuCe/PS > CuCe/CS. However, CuMn/CS had larger micro pore volume compared to CuMn/PS which can be observed as the factor responsible for the high NO removal. This finding agreed closely with Gao et al. (2011) who deduced that micro pore acted as a nano-reactor for SCR catalysts while the total BET surface area of the activated carbon did not play important role in the reaction [20]. Other studies including by Pasel et al. (1998) and Singh et al. (2013) also did not find any direct relation between the BET surface area and pore volume with the NO_x reduction but rather suggested that the surface chemical characteristic was far more important [4] [21].

3.3. X-Ray Diffraction Analysis

The coupled catalysts at nano-size impregnated on the different precursors were responsible for the reduction of NO_x and the crystallinity can be examined using the XRD which spectra are shown in Figure 3. The strong peaks at 35.5° and 38.5° as well as the weak peaks at 49.0° were ascribed to CuO catalyst which can be seen in all catalysts. This was consistent with the findings by Archana Patel et al. (2014) [22]. The convoluted peaks from 34.5° to 37.5° can be attributed to the presence of MnO species which can only be seen in Figure 3(a). De Fang et al. (2015) also reported the peaks at 40.6° and 58.7° were of the MnO phase but appeared to be weak in this study for CuMn/CS and CuMn/PS [23]. The XRD pattern for Cu-Ce coupled catalysts in Figure 3(b) showed the evolution of peak at 28° that Boxiong Shen et al. (2015) attributed to the CeO₂ catalyst [24].

It was evident that only CuMn/PS retained the characteristic curve of the carbon structure between peaks 15° to 30° compared to the other catalysts and it was the only catalyst that had no strong peak correlated to the crystalline metals. This was due to the high metal dispersion within the amorphous palm kernel carbon and showed that Cu-Mn catalysts did not destroy the carbon structure or bonding as suggested by Chu Yinghao et al. (2015) [25].

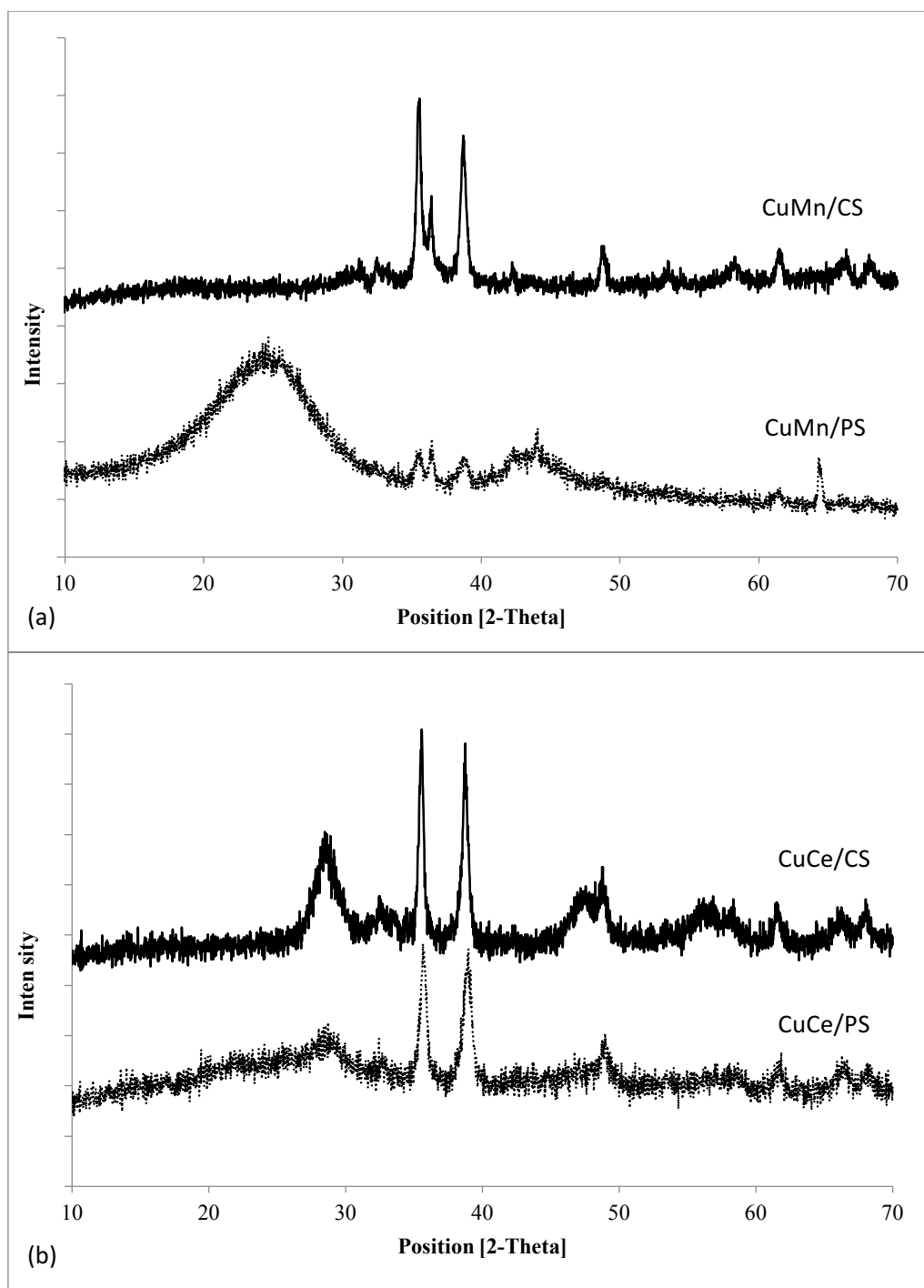


Figure 3: X-ray diffraction patterns for (a) CuMn-based catalysts (b) CuCe-based catalysts.

3.4. X-Ray Fluorescence Analysis

The intrinsic metal content of CSAC and PSAC is shown in Table 3 and the standard deviation in the brackets implies the distribution of the metal on the catalyst surface [26]. It can be noted that the main inorganic elements in CSAC were K and Ni while in PSAC were Si, Al and Fe. The decrease in these elements can be attributed to the ion exchange phenomenon with the metallic catalysts [27].

Table 3: Stoichiometric composition of inorganic elements in CSAC, PSAC, CuMn/CS, CuCe/CS, CuMn/PS, CuCe/PS.

Inorganic element	Weight (%), deviation (%)					
	CSAC	CuMn/ CS	CuCe/ CS	PSAC	CuMn/ PS	CuCe/ PS
SiO ₂	-	-	-	53.302	18.915	22.856
Al ₂ O ₃	-	-	-	18.360	-	-
K ₂ O	78.526	1.069	1.134	5.544	4.051	3.588
Fe ₂ O ₃	2.4571	-	-	16.434	0.799	-
Ni	16.0513	-	-	-	-	-
Cr	2.9653	-	-	-	-	-
CuO		80.862 (0.073)	78.224 (0.069)	-	69.581 (0.061)	63.473 (0.063)
CaO	-	0.634	0.810	2.115	1.738	-
TiO ₂	-	-	-	1.915	-	-
SO ₃		2.080	-	-	1.237	2.074
CeO ₂	-	-	16.763 (0.065)	-	-	6.213 (0.046)
MnO	-	15.356 (0.033)	-	-	3.678 (0.017)	-

Potassium, nickel, aluminum and iron contents were highly decreased after the impregnation while silicon was only reduced not more than 70% of its initial content. This showed that lower oxidation number of inorganic elements intrinsically present in the activated carbon tended to exchange ion with the transition metals. The more exchange of the elements promoted a higher metal loading which contributed to the increase in NO_x adsorption. This was especially true when correlating the high ion exchange (and metal loading) in CuMn/CS with its high total NO_x removal.

The intrinsic metal content also played important role in the dispersion of nano catalysts. Generally in Table 3, both bimetal catalysts dispersed with good distribution as the standard deviation values were lower than 1.0 but the metal loading was different between the two precursors. Catalysts impregnated onto PSAC had better distribution but the loading was lower than the catalysts derived from CSAC. The lower metal loading was a result of low ion exchange and was responsible for the low NO_x removal by CuMn/PS and CuCe/PS [4]. Nevertheless, CuCe/CS possessed the lowest NO_x removal even though the metal loading and dispersion were high which meant the removal of NO_x by the CSAC-derived catalysts were contributed by other factors such as the acidic groups.

3.5. Hydrogen Temperature-Programmed Reduction Analysis

The reduction temperature for the derived catalysts was determined using the H₂-TPR and Figure 4 shows the TPR profile for the catalysts. The reduction activity between 150 and 300 °C was credited to the pure CuO where in this experiment the maxima occurred at temperature around 300 °C [28]. At 614 °C, a broad peak was detected showing a high MnO reduction activity in CuMn/PS. This was in correlation with Kanaparthi Ramesh et al. (2007) where they determined that the activity for the MnO did not occur until 900 K [29]. Activity around 515 and 622 °C can be assigned to the CeO₂ as it was coupled with copper. However, singular CeO₂ catalysts would reduce the hydrogen at around 554 °C [8].

It can be noted that the consumption of hydrogen indicates the reduction activity [30]. At low temperature around 250 - 300 °C, CuMn/CS, CuCe/CS and CuCe/PS showed a high reduction activity which meant the catalysts were reactive at low temperature. When incorporated with the coconut shell carbon, the Cu-Mn catalyst consumed more hydrogen than the CuCe/CS. However, it became less reactive when deposited on PSAC which can be seen from Figure 4(c) where less than 15% of hydrogen was consumed at 250 °C but 77% was consumed at 614 °C.

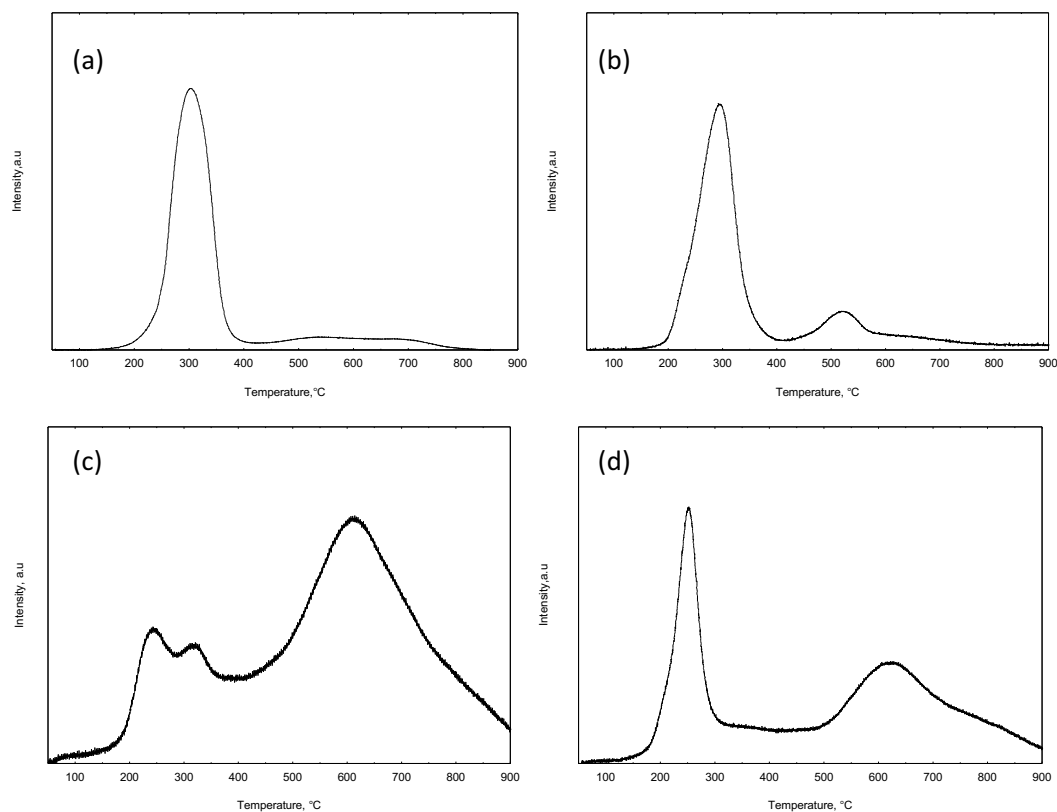


Figure 4: Hydrogen temperature-programmed reduction of (a) CuMn/CS (b) CuCe/CS (c) CuMn/PS (d) CuCe/PS.

3.6. Fourier-Transform Infra-Red Analysis

The surface acid-base property was characterized using the FTIR. Oxygenated functional groups such as carboxyl, ethers and lactones are preferred to be present in an SCR catalyst to anchor the metallic catalysts and to adsorb NO_x gases for the reaction to occur [31]. Figure 5 displays the change in the intensity of the functional groups as the CSAC and PSAC were impregnated with different bimetallic catalysts.

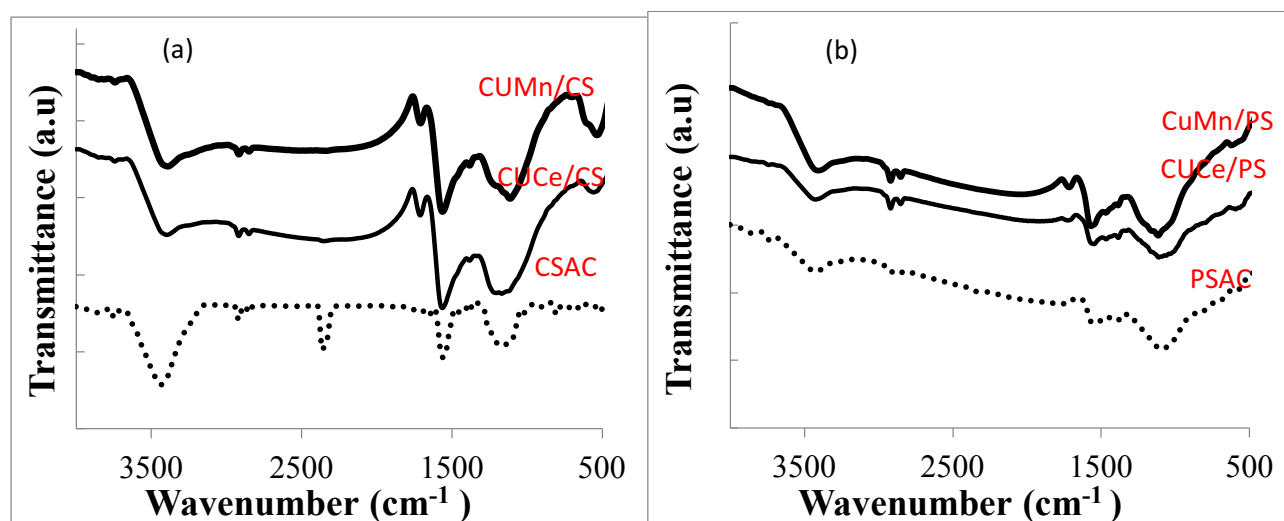


Figure 5: Fourier-Transform Infra-Red spectra for (a) CSAC, CuMn/CS and CuCe/CS; (b) PSAC, CuMn/PS and CuCe/PS.

It can be seen from Figure 5(a) that the intensity of –OH stretch from 3650 to 3170 cm^{-1} in CuMn/CS and CuCe/CS was lower than their support showing the used-up of the alcohol functional groups. The $\text{C}\equiv\text{C}$ bond at around 2360 cm^{-1} also disappeared after the impregnation of the bimetallic. On the other hand, the ketone group at peak 1710 cm^{-1} appeared and the amine group at around 1600 cm^{-1} increased in the intensity after the impregnation which can increase the NO_x removal. This was an equivalent case for both CuMn/CS and CuCe/CS exhibiting their similarity in the surface acidity but the reduction capability of CuMn/CS was higher than CuCe/CS (see Section 3.5).

Figure 5(b) shows that PSAC and its catalysts possessed less oxygenated functional groups in comparison to CSAC. Nevertheless, the same pattern of bonds-breaking and used-up can be observed after the impregnation stage. Both of the PSAC-derived catalysts exhibited identical FTIR spectra showing their similar surface acidity which explained the almost similar performance in removing NO_x gases.

Conclusions

The highest total NO_x removal was 74%, achieved by CuMn/CS catalyst at 250 °C and the lowest performance was attained by CuCe/CS which gave only 42%. Besides, CuMn/CS gave high NO removal while CuMn/PS adsorbed the highest amount of NO_2 . In the characterization, it was found that CuMn/CS had the highest micro pore volume while CuCe/CS had the least among all catalysts used in this study. However, all nano catalysts displayed a high crystallinity except for CuMn/PS where the catalyst could have been deeply dispersed into the micro structure of the palm kernel carbon. This did not affect the performance of the catalyst as it was shown that CuMn/PS was able to remove more NO_x compared to CuCe/CS. In the XRF analysis, CuMn/PS showed a high catalysts distribution over the carbon surface and considerably good loading. This analysis also exhibited that the intrinsic metal content of the carbon had major role in determining the loading and distribution of the nano catalysts over the surface. H_2 -TPR experiment suggested that all catalysts except CuMn/PS were reactive at low temperature. The FTIR analysis displayed the change in the oxygenated functional groups after the catalysts impregnation. In addition, it is worth to mention that Cu-Mn was best to be incorporated over the coconut shell carbon while Cu-Ce over the palm kernel shell carbon. As a conclusion, the NO_x removal percentage of the catalysts in this study showed that the agro-waste can be further developed as SCR catalyst support. It is recommended that the actual performance of the catalyst in an SCR system be explored.

Acknowledgments—The authors acknowledge the Ministry of Higher Education Malaysia for the fund FRGS/TK04(02)/1138/2014(05) as well as Universiti Malaysia Sarawak and Universiti Putra Malaysia for the research facilities.

References

1. Chandrasekaran M., Bahkali A., *Saudi J. Biol. Sci.* 20 (2013) 105.
2. Food and Agriculture Organization of the United Nations, *FAOSTAT* 2015. [Online]. Available: <http://faostat3.fao.org/browse/FB/BC/E>. [Accessed 10 December 2015].
3. Rashidi N., Yusup S., Ahmad M., Mohamed N., Hameed B., *APCBEE Procedia* 3 (2012) 84.
4. Singh S., Nahil M., Sun A., Wu C., Shen B., Williams P., *Fuel* 105 (2013) 585.
5. Arve K., Svennerberg K., Klingstedt F., *J. Phys. Chem. B* 110 (2006) 420.
6. Wang Z., Yamaguchi M., Goto I., Kumagai M., *Physical Chem. Chemical Phys.* 2 (2000) 3007.
7. Sessa S., Prakash C., *Catalysts* 2 (2012) 434.
8. Lei C., Duan W., Zhichun S., Xiaodong W., *Prog. Nat. Sci: Mater. International* 22 (2012) 265.
9. Qiu M., Zhan S., Yu H., Zhu D., Wang S., *Nanoscale* 7 (2015) 2568.
10. Thirupathi B., Smirniotis P. G., *Appl. Catal. B: Environ.* 110 (2011) 195.
11. Xu H., Wang Y., Cao Y., Fang Z., Lin T., Gong M., Chen Y., *Chem. Eng. J.* 240 (2014) 62.
12. Yin C., Wang L., Rivillon S., Shih A. J., Yang R. T., *Catal. Lett.* 145 (2015) 1491.
13. More P. M., Nguyen D. L., Granger P., Dujardin C., Dongare M. K., Umbarkar S. B., *Appl. Catal. B: Environ.* 174 (2015) 145.
14. Lindholm A., Sjovalld H., Olsson L., *Appl. Catal. B: Environ.* 98 (2010) 112.
15. Li J., Wang S., Zhou L., Luo G., Wei F., *Chem. Eng. J.* 255 (2014) 126.

16. Wang A., Ma L., Cong Y., Zhang T., Liang D., *Appl. Catal. B: Environ.* 40 (2003) 319.
17. Ibrahim Y., Norsuzailina M., Yun-Hin T. Y., Md S., *WIT Trans. Energy Sustain.* 189 (2014) 291.
18. Muniz J., Marban G., Fuertes A., *Appl. Catal. B: Environ.* 27 (2000) 27.
19. Bingnan F., Guanzhoung L., Yanqin W., Yun G., Yanglong G., *Chin. J. Catal.* 32 (2011) 853.
20. Gao X., Liu S., Zhang Y., Du X., Luo Z., Cen K., *Catal. Today* 175 (2011) 164.
21. Pasel J., KaBner P., Montanari B., Gazzano M., Vaccari A., Makowski W., Lojewski T., Dziembaj R., Papp H., *Appl. Catal. B: Environ.* 18 (1998) 199.
22. Archana P., Pradeep S., Thomas E. R., Victor R., Zhonghua Z., *Chem. Eng. J.* 255 (2014) 437
23. Fang D., Xie J., Hu H., Yang H., He F., Fu Z., *Chem. Eng. J.* 271 (2015) 23.
24. Shen B., Chen J., Yue S., Li G., *Fuel* 156 (2015) 47.
25. Yinghao C., Tengting Z., Jiaxiu G., Chao L., Huaqiang Y., Xiaofan Z., Yongjun L., *J. Rare Earth* 33 (2015) 371.
26. Thakur D., Tiggelaar R., Gardeniers J., Lefferts L., Seshan K., *Chem. Eng. J.* 227 (2013) 128.
27. Garcia-Bordeje E., Monzon A., Lazaro M. J., Moliner R., *Catal. Today* 102 (2005) 177.
28. Ouzzine M., Cifredo G. A., Gatica J. M., Harti S., Chafik T., Vidal H., *Appl. Catal. A: General* 342 (2008) 150.
29. Kanaparthi R., Luwei C., Fengxi C., Yan L., Zhan W., Yi-Fan H., *Catal. Today* 131 (2008) 477.
30. Xin G., Ming L., Jianyi S., *J. Solid State Chem.* 161 (2001) 38.
31. Lu P., Li C., Zeng G., He L., Peng D., Cui H., Li S., Zhai Y., *Appl. Catal. B: Environ.* 96 (2010) 157.

(2016); <http://www.jmaterenvirosci.com>